Effects of hemicelluloses on dehydrogenative polymerization of monolignols with cationic cell wall-bound peroxidase

*Yan Lyu[a], Shiori Suzuki[b], Hiroki Nagano[a], Kengo Shigetomi[b], Yutaka Tamai[b], Yuji Tsutsumi[c], Yasumitsu Uraki[b]**

[a] Graduate School of Agriculture, Hokkaido University, Sapporo 060-8589, Japan

[b] Research Faculty of Agriculture, Hokkaido University, Sapporo 060-8589, Japan

[c] Faculty of Agriculture, Kyushu University, Fukuoka 812-8581, Japan

*To whom correspondence may be addressed. Email: uraki@for.agr.hokudai.ac.jp

Abstract

To elucidate the influence of polysaccharides on hardwood lignification, dehydrogenative polymerization of monolignols, coniferyl alcohol (CA) and sinapyl alcohol (SA), was attempted with recombinant cationic cell wall-bound peroxidase (rCWPO-C) and horseradish peroxidase (HRP) in measurement cells of a quartz crystal microbalance with dissipation (QCM-D). Hardwood cellulose nanofibers were anchored; hemicelluloses, xylan, partially acetylated xylan (AcXY), galactoglucomannan, and xyloglucan, and the enzymes were subsequently adsorbed onto the QCM-D sensor surface, enabling fabrication of artificial polysaccharide matrices. The largest amount of rCWPO-C is found to be adsorbed onto AcXY among all the polysaccharides, which affords the largest amount and size of spherical dehydrogenation polymers (DHPs) from both CA and SA. In contrast, no DHP and a small amount of DHPs are formed from SA and CA, respectively, by HRP catalysis in all of the polysaccharide matrices. This study demonstrates important functions of a real tree-derived peroxidase, rCWPO-C, and AcXY for hardwood lignification.

Keywords: Dehydrogenation polymer; sinapyl alcohol; cationic cell wall-bound peroxidase; hemicellulose; partially acetylated xylan.

Abbreviations: AcXY, partially acetylated WXY; CA, coniferyl alcohol; CNFs, hardwood cellulose nanofibers; DHP, dehydrogenation polymers; 2,6-DMP: 2,6-dimethoxyphenol; GGM, galactoglucomannan; HRP, horseradish peroxidase; QCM-D, a quartz crystal microbalance with dissipation; rCWPO-C, recombinant cationic cell wall-bound peroxidase; SA, sinapyl alcohol; WXY, a water-soluble fraction of commercial beech xylan; XG, xyloglucan.

Introduction

Lignin is one of the major wood cell wall components, and its formation, termed lignification, occurs through radical couplings between monolignols, coniferyl alcohol (CA), sinapyl alcohol (SA), *p*-coumaryl alcohol (Ralph, Brunow, & Boerjan, 2007), and/or oligolignols. Cell wall formation in trees starts with the deposition of polysaccharides, cellulose and hemicelluloses on the plasma membrane to form a polysaccharide matrix. Subsequently, lignification occurs in the matrix. Therefore, the matrix has been proposed to affect lignification with respect to the amount formed and the lignin structure. The influence of hemicelluloses on lignification has been elucidated from the spatial arrangement of cell wall components (Donaldson, 1994; Terashima, Yoshida, Hafrén, Fukushima, & Westermark, 2012; Warinowski et al., 2016; Wi, Singh, Lee, & Kim, 2005) and lignin structures in lignin-carbohydrate complexes (LCCs) isolated from wood. However, the latter investigations have suggested contradictory functions of hemicelluloses for lignification. One investigation has reported that xylan promotes the *b-O-4'* linkage as a predominant interunitary linkage of lignin (Giummarella, Zhang, Henriksson, & Lawoko, 2016), but another study has reported that glucomannan facilitates this linkage more than xylan (Du, Gellerstedt, & Li, 2013; Du et al., 2014). These opposite results should be attributed to the fact that the investigations do not directly address the lignification process.

To overcome the experimental drawback, dehydrogenative polymerization of CA was attempted as an artificial lignification by endwise polymerization (Saake, Argyropoulos, Beinhoff, & Faix, 1996) with horseradish peroxidase (HRP) as a catalyst in an artificial polysaccharide matrix, which

was fabricated by depositing commercial beech xylan on bacterial cellulose (BC) (Li et al., 2015). As a result, the xylan yielded larger amounts of dehydrogenation polymers (DHPs) with a higher frequency of *β-O-4'* linkage than cellulose. By using BC-galactoglucomannan (GGM) and BC-xyloglucan (XG) matrices, GGM was found to inhibit polymerization, while XG contributed to DHP formation with condensed structures such as lignin in primary cell walls (Lyu et al., 2021). However, these investigations still had a drawback in that the HRP used is not a tree enzyme and hardly oxidizes SA (Aoyama et al., 2002; Veitch, 2004). Thus, HRP is unsuitable for the elucidation of lignification in hardwood derived from CA and SA.

This study aims to elucidate hardwood lignification from DHP formation in artificial polysaccharide matrices by using a real tree enzyme. It has been reported that native glucuronoxylan in hardwood is partially acetylated with the degree of substitution (DS) ranging from 0.40−0.75 (Pawar, Koutaniemi, Tenkanen, & Mellerowicz, 2013; Qaseem & Wu, 2020; Teleman, Lundqvist, Tjerneld, Stålbrand, & Dahlman, 2000; Teleman, Tenkanen, Jacobs, & Dahlman, 2002). Based on this fact, we hypothesize that this acetyl (Ac) group should play an important role in hardwood lignification. However, little work has been conducted to investigate it, although many have been done for unsubstituted glucuronoxylan (Li et al., 2015; Pawar et al., 2017). In this study, a partially acetylated xylan is firstly prepared as a model of native hardwood xylan from a commercially available xylan, because this commercial xylan, extracted from beech with an alkaline aqueous solution, does not contain Ac group. Then, the water-soluble fractions of the commercial xylan and partially acetylated xylan are separately subjected to the fabrication of polysaccharide matrices. If there is a difference in the DHP formation between these polysaccharide matrices, our hypothesis would be verified.

As mentioned above, HRP is not proper to verify this, and therefore, a cationic cell wall-bound peroxidase (CWPO-C) is focused on. This enzyme was discovered in poplar (*Populus alba* L.) (Aoyama et al., 2002; Sasaki, Nishida, Tsutsumi, & Kondo, 2004) and is able to oxidize not only CA but also SA and polymeric lignin (Aoyama et al., 2002; Sasaki et al., 2004). However, it is

difficult to isolate a large quantity of CWPO-C from hardwood, and thus, recombinant CWPO-C (rCWPO-C) (Shigeto, Itoh, Tsutsumi, & Kondo, 2012) is used in this study.

This study adopts a quartz crystal microbalance with dissipation (QCM-D) to analyze the interactions between lignification-involving materials and to elucidate DHP formation (Elschner, Adam, Lesny, Joseph, & Fischer, 2022; Wang, Qian, Roman, Glasser, & Esker, 2013) because QCM-D enables measurements using a small amount of samples. Accordingly, artificial polysaccharide matrices are fabricated on the QCM-D sensor with hardwood-derived cellulose and hemicelluloses (the partially acetylated and unsubstituted xylans, GGM, and XG) prior to the real-time monitoring of DHP formation catalyzed by rCWPO-C and HRP as a reference.

2. Materials and Methods

2.1. Water-soluble fraction of commercial beech xylan (WXY) and its partially acetylated xylan (AcXY)

Commercial beech xylan (SERVA Electrophoresis GmbH, Heidelberg, Germany) was dissolved in water at room temperature (25 °C) for 1 day, and the suspension was centrifuged to obtain a water-soluble fraction as the supernatant. The water-soluble fraction was delignified with sodium chlorite according to a modified Wise method and freeze-dried to yield WXY. The sugar constituents of WXY were 76.8% xylose, 7.3% glucose, 12.8% glucuronic acid, 0.3% Klason lignin, and 0.7% acid soluble lignin (Lyu et al., 2021).

WXY (5 g) was suspended in *N,N*-dimethylacetamide (50 mL) with stirring at 120 °C for 16 h, and then LiCl (3.76 g) was added to the suspension. The mixture was stirred at 80 °C for approximately 16 h until WXY was completely dissolved. Methane sulfonic acid (2.5 mL) and acetic anhydride (32.5 mL) were added to the solution, and the mixture was stirred at 80 °C for 16 h. The resultant solution was slowly poured into distilled water. The precipitate was collected by filtration, rinsed with distilled water, and then dried *in vacuo* overnight to yield fully acetylated WXY with a yield of 78% based on the theoretical output value.

The fully acetylated WXY (1 g) was dissolved in chloroform (100 mL) with stirring at room temperature. Sodium methoxide (2.4 g) was then added to the solution and stirred at room temperature for 16 h. The solution was neutralized with acetic acid and then dialyzed against distilled water for 3 days. The water was changed every 4 h during the daytime. The dialyzed suspension was evaporated to the solid and dried *in vacuo* at 50 °C for 2 days. The resultant solid (0.22 g) was suspended again in 50 mL of water for 16 h, and the supernatant was collected by centrifugation. It was lyophilized to give the water-soluble fraction (AcXY). The AcXY formed 65% of the total weight of the partially deacetylated derivative of fully acetylated WXY.

The degree of substitution (DS) of fully acetylated WXY and AcXY was determined by a titration method (Taira et al., 2020) and FT-IR measurements (see Fig. S1 for details of the DS determination). ^{1}H-/^{13}C-NMR spectra for WXY and AcXY were measured in deuterated dimethylsulfoxide (DMSO-d_6) or deuterium oxide using a 500 MHz spectrometer (Bruker AVANCE Neo, Billerica, United States). The chemical shift of the deuterated solvent was used as a reference (δ = 2.49 ppm) for ^{1}H-NMR. The molar mass distributions of WXY and AcXY were measured by using a size exclusion chromatography (SEC) system (see Supporting Information for the detail conditions).

2.2. Other polysaccharides

A hydrogel of cellulose nanofibers (CNFs) derived from hardwood kraft pulp was provided by Hokuetsu Corporation (Tokyo, Japan). The gel was diluted to approximately 1/5 consistency and dialyzed against distilled water for 3 days. The dialyzed CNF suspension was concentrated to 0.74 g/L by evaporation. The composition of the CNFs was 72.5% glucose, 16.8% xylose, and 0.5% Klason lignin (Lyu et al., 2021).

Crude glucomannan was extracted and purified according to a previous report (Lyu et al., 2021). The obtained glucomannan (GGM) was composed of 13.7% glucose, 39.4% galactose, 41.1% mannose, 0.1% Klason lignin, and 0.9% acid soluble lignin.

Xyloglucan (XG) extracted from tamarind seed was purchased from Megazyme (Ireland) and used as received. XG was composed of 47.9% glucose, 24.9% xylose, 1.8% arabinose, 18.5% galactose, 0.9% Klason lignin, and 1.2% acid-soluble lignin (Lyu et al., 2021).

2.3. Enzyme activity measurement

rCWPO-C preparation and purification procedures were conducted using the same method as reported previously (Shigeto et al., 2012). HRP was purchased from FUJIFILM Wako Pure Chemical Industries (Osaka, Japan) and used as received. The enzyme activity of rCWPO-C and HRP (Shigeto et al., 2012) was measured at 25 °C on the basis of the oxidation of guaiacol and 2,6-dimethoxyphenol (2,6-DMP) in Tris-HCl (50 mM, pH 7.5) buffered solution and phosphate buffered saline (PBS, pH 6.1, 0.01 M phosphate containing 0.8 w/v% NaCl and 0.02 w/v% KCl), respectively. The absorbance of the enzymatic oxidation products (i.e., tetraguaiacol and coerulignone from guaiacol and 2,6-DMP, respectively) were monitored at a wavelength of 470 nm and 469 nm, respectively, using a UV–vis absorption spectrophotometer (U-3310, HITACHI High-Tech Science, Kyoto, Japan).

Enzyme activity (A U/mg) based on the generation of the product within 1 min after H_2O_2 addition was calculated by using the following equation (Shigeto et al., 2012; George, 1953; Wariishi et al., 1992):

$$A = \frac{(\Delta E_1 - \Delta E_2) \times v}{\varepsilon \times c \times v_0}$$

where ΔE_1 is the rate of increase in absorbance (per min) of the reaction solution, ΔE_2 is the rate of increase in the absorbance (per min) of the blank solution, v is the total volume of the reaction mixture, c is the enzyme concentration, and v_0 is the volume of the added enzyme solution. ε is the absorptivity of the oxidation product and is equal to 26.6 L/mmol/cm for tetraguaiacol (George, 1953) and 49.6 L/mmol/cm for coerulignone (Wariishi, Valli, & Gold, 1992).

2.4. QCM-D measurements

A CNF-coated QCM-D sensor was prepared according to our previous report (Lyu et al., 2021). The frequency change (Δf) of the sensor before and after CNF deposition was measured using a QCM-D (Q-sense AB, Biolin Scientific, Västra Frölunda, Sweden). The dried amount of CNFs deposited onto the sensor was calculated by using the Sauerbrey equation (Sauerbrey, 1959):

$$\Delta m = C(\Delta f/n)$$

where Δm (ng/cm^2) is the weight change, C is the mass sensitivity constant of the sensor (-17.7 ng/cm^2/Hz), and n is the overtone number (n = 5 in this study). For a Δm of less than 4000 ng/cm^2, the CNF coating was further repeated until Δm exceeded 4000 ng/cm^2, at which point the CNFs theoretically covered the whole surface of the sensor as a monolayer (Lyu et al., 2021; Sugiyama, Vuong, & Chanzy, 1991).

The dried CNF-coated sensor was set in a measurement cell and conditioned with a flow of Mill-Q water. Then, a hemicellulose solution at 1 mg/mL was introduced into the cell for 2 h. Mill-Q water was subsequently introduced for 15 min to remove unbound hemicellulose. All QCM-D measurements were performed at 25 °C, and the flow rate for all solutions was controlled to be 50 µL/min by using a peristaltic pump (ISM795C, Iamatec^{TM}, Fisher Scientific, Sweden). The changes in the Δf and dissipation factor (ΔD) of the sensor were monitored during measurements. The dissipation factor (D) is defined by the following equation (Dixon, 2008):

$$D = \frac{E_{diss}}{2\pi E_{stored}}$$

where E_{diss} is the dissipated energy and E_{stored} is the stored energy during one oscillation.

After the hemicellulose adsorption process, Mill-Q water in the cell was exchanged with Tris-HCl or PBS buffered solutions. Then, an enzyme buffered solution (rCWPO-C in a Tris-HCl buffered solution or HRP in a PBS buffered solution) at a concentration of 5 U/mL for guaiacol was introduced at 50 µL/min for 30 min. After the adsorption experiment, the sensor surface was rinsed

with the buffered solution for 15 min. This enzyme adsorption was also conducted on the water-swelled CNF-coated sensor without hemicelluloses.

CA and SA were synthesized according to the same method as reported previously (Quideau & Ralph, 1992). After enzyme adsorption, a monolignol (2.7 mM) buffered solution containing H_2O_2 (2.7 mM) was introduced into the cell for 1 h. The sensor surface was successively rinsed with the corresponding buffer solution for 15 min and Milli-Q water for 30 min and subjected to the following observation. As a reference, monolignol adsorption was conducted for a CNF-coated sensor without H_2O_2 after enzyme adsorption. Each measurement was repeated at least two times until the same trend profiles were obtained.

2.5. Atomic force microscope (AFM) imaging

The sensors used for DHP formation were dried under a N_2 flow and observed using AFM (SPA-400 AFM, HITACHI High-Tech Science, Kyoto, Japan). Images of the sensor surfaces were taken in tapping mode using a SI-DF-40 cantilever (HITACHI High-Tech Science, Kyoto, Japan) and expressed as shape images. The mean surface roughness (Ra) over a scan area of 2.5×2.5 μm^2 was estimated by using Gwyddion software.

3. Results and Discussion

3.1. Preparation and characterization of AcXY

WXY was fully acetylated under homogeneous conditions and then deacetylated using sodium methoxide to yield partially acetylated xylan with a DS of 0.50 (see Fig. S1 for the DS determination), which is close to the DS of native xylan in hardwood (Pawar et al., 2013; Teleman et al., 2000; Teleman et al., 2002). Its water-soluble fraction was collected to yield AcXY with a similar DS to that obtained before fractionation. The size exclusion chromatograms of WXY and AcXY are shown in Fig. S2 and Table S1. As WXY shows a bimodal chromatogram (Lyu et al.,

2021), AcXY also shows a similar chromatogram, but the peak in the low molar mass range was slightly shifted toward the lower molar mass region than that of WXY.

The distribution of acetyl (Ac) groups in AcXY was analyzed by using ^{1}H- and ^{13}C-NMR (Fig. 1 and Fig. S3, respectively). The ^{1}H-NMR spectrum shows chemical shifts at 2.17 and 2.15 ppm, which are assigned to the methyl protons of the Ac group at the C-2 position (Xyl-2Ac) and C-3 position (Xyl-3Ac), respectively (Zhong, Cui, & Ye, 2017), and their integral ratio is approximately 1:1. No chemical shift for the Ac groups at both the C-2 and C-3 positions (Xyl-2,3Ac) was observed. These results suggest that the Ac group is located at either the C-2 or C-3 position in each anhydroxylose unit of AcXY. Thus, a partially acetylated xylan (i.e., AcXY) was successfully prepared as the model of native hardwood xylan for the following investigations.

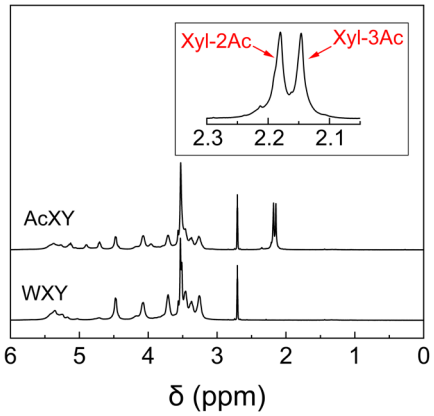

Fig. 1. ^{1}H-NMR spectra for AcXY and WXY in DMSO-d_6. An expanded spectrum of AcXY shows the assignments for the methyl protons of the Ac groups.

3.2 Hemicellulose adsorption on CNFs

In our previous report (Lyu et al., 2021), hemicellulose adsorption on cellulose was monitored using a QCM-D, and the adsorption amount followed the order of XG > GGM > WXY. In this study, the AcXY adsorption on CNFs was further investigated by using the QCM-D. It should be noted that the CNFs used in this study were derived from hardwood kraft pulp, thus, originally containing a small amount of xylan (*ca*. 17%).

Figure 2 shows two types of QCM-D profiles for AcXY: Δ*f*/n versus elution time (Fig. 2a) and Δ*D* versus Δ*f*/*n* (Δ*D*-Δ*f*/n plot, Fig. 2b), where the profiles for WXY are depicted as a reference (Lyu et al., 2021). Δ*f*/n exhibits the adsorption amount of AcXY and WXY on the CNF-coated sensor, and a smaller Δ*f*/n corresponds to a larger adsorbed amount. The Δ*D*-Δ*f*/n plot reflects the viscoelastic change in the adsorbed layer on the sensor; a steep curve indicates that the surface layer becomes viscous or soft, whereas a gradually increasing curve indicates that the surface becomes elastic or rigid (Littunen, Mai-Gisondi, Seppälä, & Master, 2017).

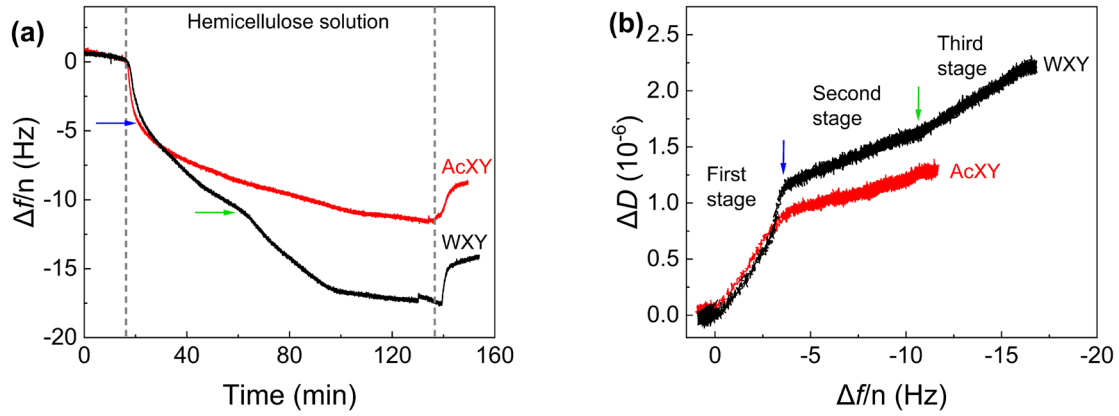

Fig. 2. QCM-D profiles for frequency change (Δ*f*/n) as a function of elution time (a) and dissipation change (Δ*D*) as a function of Δ*f*/n (b) during adsorption of AcXY and WXY on the CNF-coated sensor. The blue and green arrows show the border for each stage.

As shown in Fig. 2b, the Δ*D*-Δ*f*/n profile for AcXY can be divided into two stages: the first stage ranges from 0 to -4 Hz, and the second stage ranges from -4 to -11 Hz. On the other hand, the

profile for WXY can be divided into three stages: the first and second stages are located in the same ranges as those for AcXY, but the third stage appears from -11 to -17 Hz.

In the first stage, the Δ*f*/n profiles for AcXY and WXY (Fig. 2a) are almost identical, with Δ*f*/n showing a rapid decrease, indicating the rapid adsorption of AcXY and WXY onto the CNF surface. Concomitantly, Δ*D* also rapidly increases, suggesting that the sensor surfaces become soft due to the adsorption of hydrated AcXY and WXY. In the second stage, the Δ*f*/n for AcXY and WXY gradually decreases, and the slope of the Δ*D*-Δ*f*/n plot becomes less steep than that in the first stage, indicating that the surface becomes relatively rigid. This phenomenon can be attributed to the release of bound water from hydrated AcXY and WXY to achieve further adsorption of the hemicelluloses on CNFs (Farooq et al., 2020). Furthermore, the rate of decrease of Δ*f*/n for WXY in the second stage is faster than that for AcXY. Such rapid adsorption of WXY can be promoted via much hydrogen bonding interactions with CNFs compared with AcXY.

At the third stage of WXY, Δ*f*/n shows a rapid decrease followed by a gradually decrease. The Δ*D*-Δ*f*/n plot for WXY also changes to a steeper slope than that in the second stage. These results suggest that the formed layer becomes soft through a different mode of adsorption. It has been reported that xylan without substituents tends to self-associate (Eronen, Österberg, Heikkinen, Tenkanen, & Laine, 2011; Kabel, van den Borne, Vincken, Voragen, & Schols, 2007). Thus, the softer layer formed in the third stage can be attributed to the self-association of WXY, resulting in a maximum adsorption on CNFs. In contrast, the total amount of AcXY adsorbed on CNFs is smaller than that for WXY because the Ac group in AcXY can inhibit self-association.

3.3. Enzyme activity and adsorption on polysaccharides

The oxidation activities of rCWPO-C and HRP were determined with guaiacol and 2,6-DMP as model substrates for CA and SA, respectively. rCWPO-C shows a high activity of 432 U/mg for 2,6-DMP, which is approximately three times higher than the activity of 148 U/mg for guaiacol. On the other hand, HRP shows an extremely low activity of 177 U/mg for 2,6-DMP, which is only 0.35

265 times the activity of 503 U/mg for guaiacol. Therefore, rCWPO-C is confirmed to have a high ability
266 to oxidize syringyl nuclei (Aoyama et al., 2002; Shigeto et al., 2012).

267 The enzyme solution at 5 U/mL for guaiacol oxidation was flowed into the QCM-D sensor coated
268 with polysaccharides, and the time course for the enzyme adsorption was monitored by using QCM-
269 D. In this measurement, the CNFs were used as a reference material to evaluate the effect of each
270 hemicellulose on rCWPO-C adsorption. rCWPO-C shows the largest adsorption amount on AcXY
271 among the polysaccharides used in this study (Fig. 3), whereas the adsorption amount of HRP on
272 AcXY is less than that on CNFs (Fig. S2). rCWPO-C is more hydrophobic than HRP (Aoyama et
273 al., 2002), and the acetylation of xylan increases the hydrophobicity (Busse-Wicher et al., 2014).
274 Therefore, it is considered that rCWPO-C adsorption on AcXY can be enhanced via hydrophobic
275 interactions.

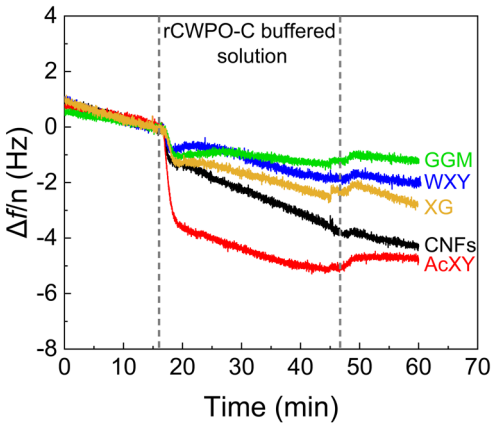

276

277 **Fig. 3.** Δ*f*/n profiles as a function of elution time for rCWPO-C adsorption on polysaccharide-coated
278 sensors.

279

280 ***3.4. DHP formation in artificial wood cell wall polysaccharide matrices***

281 DHP formation from CA was attempted in HRP-adsorbed QCM-D sensors coated with CNFs by
282 flowing CA solution with/without H_2O_2 (Wang et al., 2013). As shown in Figs. 4a and -e, there is a
283 difference of 7 Hz between the maximum absolute values for Δ*f*/n (|Δ*f*/n|) in the presence and
284 absence of H_2O_2. After the QCM-D measurement with H_2O_2, the AFM image of the sensor surface

285 (Fig. 5b) shows the presence of small particles on the fibrous CNFs, indicating DHP formation from
286 CA on the CNF-coated sensor by HRP catalysis. Furthermore, for the cases with H_2O_2, all the
287 maximum $|\Delta f/n|$ values for the other polysaccharide-coated sensors are higher than that for the CNF-
288 coated sensor without H_2O_2, suggesting that more DHPs are formed. In particular, the largest $|\Delta f/n|$
289 value is recorded for the AcXY-coated sensor, where DHP particles are also observed by AFM (Fig.
290 5c). These results imply that AcXY facilitates DHP formation from CA. On the other hand, when
291 the SA solution is flowed (Figs. 4b,f), all $|\Delta f/n|$ values are almost constant regardless of the presence
292 or absence of H_2O_2 and the type of polysaccharides used for coating the sensors. Considering the
293 decrease in $\Delta f/n$ at the beginning of the SA flow, DHP is not formed from SA due to the low activity
294 of HRP for syringyl nuclei (Wang et al., 2013), and only SA adsorption proceeds on the sensor
295 surface.

296 For CA flow into the rCWPO-C-adsorbed sensor coated with CNFs (Figs. 4c,e), there is a
297 larger difference of 58 Hz between the maximum $|\Delta f/n|$ in the presence and absence of H_2O_2 than
298 that for HRP-adsorbed sensors, suggesting the superior DHP formation of rCWPO-C from CA
299 compared to that of HRP. The AFM images of the resultant sensor surfaces (Figs. 5d,e) clearly show
300 the DHP particles formed and adsorbed along the fibers. The highest $|\Delta f/n|$ in the presence of H_2O_2
301 is recorded on the AcXY-coated surface among all polysaccharides. This can be explained by not
302 only the higher adsorption amount of rCWPO-C on AcXY than on other polysaccharides but also
303 the hydrophobicity of AcXY.

304 When the SA/H_2O_2 solution is flowed (Figs. 4d,f), the maximum $|\Delta f/n|$ values in all
305 polysaccharide matrices are 3−12 times larger than those obtained from the CA/H_2O_2 solution in
306 the corresponding matrices because of the superior oxidation activity of rCWPO-C for syringyl
307 nuclei compared to that for guaiacyl nuclei (Aoyama et al., 2002; Shigeto et al., 2012). In particular,
308 the AcXY-coated sensor exhibits the highest $|\Delta f/n|$, which is six times higher than that for CA. The
309 AFM image of the sensor (Fig. 5g) shows many particles with larger diameters of several hundred
310 nanometers, and the particles completely cover the sensor surfaces. The formation of “sphere”

311 nanoparticles of lignin and DHP from monolignols has been also confirmed in previous research
312 (Terashima et al., 2012; Chao et al., 2013). Although the mechanism to form globular lignin in wood
313 cell walls has not been clarified yet, Terashima et al. assumed that it would be a micellar aggregate
314 of oligolignols folded at the *β-O*-4 bond with their phenolic ends on the outer part of the aggregate.
315 The formation of globular lignin in the early stages of lignification is a very important phenomenon,
316 and the detailed mechanism is a subject for our further investigation.

317 As shown in Figs. 5f, g and Fig. S3 of AFM images of the sensors coated with other
318 polysaccharides, this study clearly demonstrates that rCWPO-C catalyzes the formation of a large
319 amount and size of spherical DHPs from SA in all polysaccharide matrices. Furthermore, this
320 tendency is the most significant for AcXY among all polysaccharides. These results suggest the Ac
321 group in xylan plays an important role in hardwood lignification, verifying our hypothesis.

322 For other polysaccharides, XG was found to promote DHP formation from SA catalyzed by
323 rCWPO-C followed by AcXY, as shown in Fig. 4d, although WXY and GGM are comparable to
324 CNFs. Thus, XG should be an important polysaccharide for lignification in the primary cell walls
325 of hardwood. On the other hand, WXY promotes DHP formation from CA catalyzed by rCWPO-C
326 and HRP compared with XG, GGM, and CNFs, implying that the xylan backbone itself may also
327 be related to lignification.

328 DHP formation from CA in unsubstituted polysaccharide matrices has been examined in our
329 previous studies using HRP, which revealed significant effects of WXY and XG on the amount and
330 structure of the generated DHPs (Li et al., 2015, Lyu et al., 2021). However, this is the first study to
331 demonstrate the significance of Ac groups on present in hardwood xylan through DHP formation
332 from both CA and SA catalyzed by a real tree enzyme, rCWPO-C. As galactoglucomannan in
333 softwood also contains a small amount of Ac group (Willför, Sundberg, Tenkanen, & Holmbom,
334 2008), its function will be further investigated to understand softwood lignification.

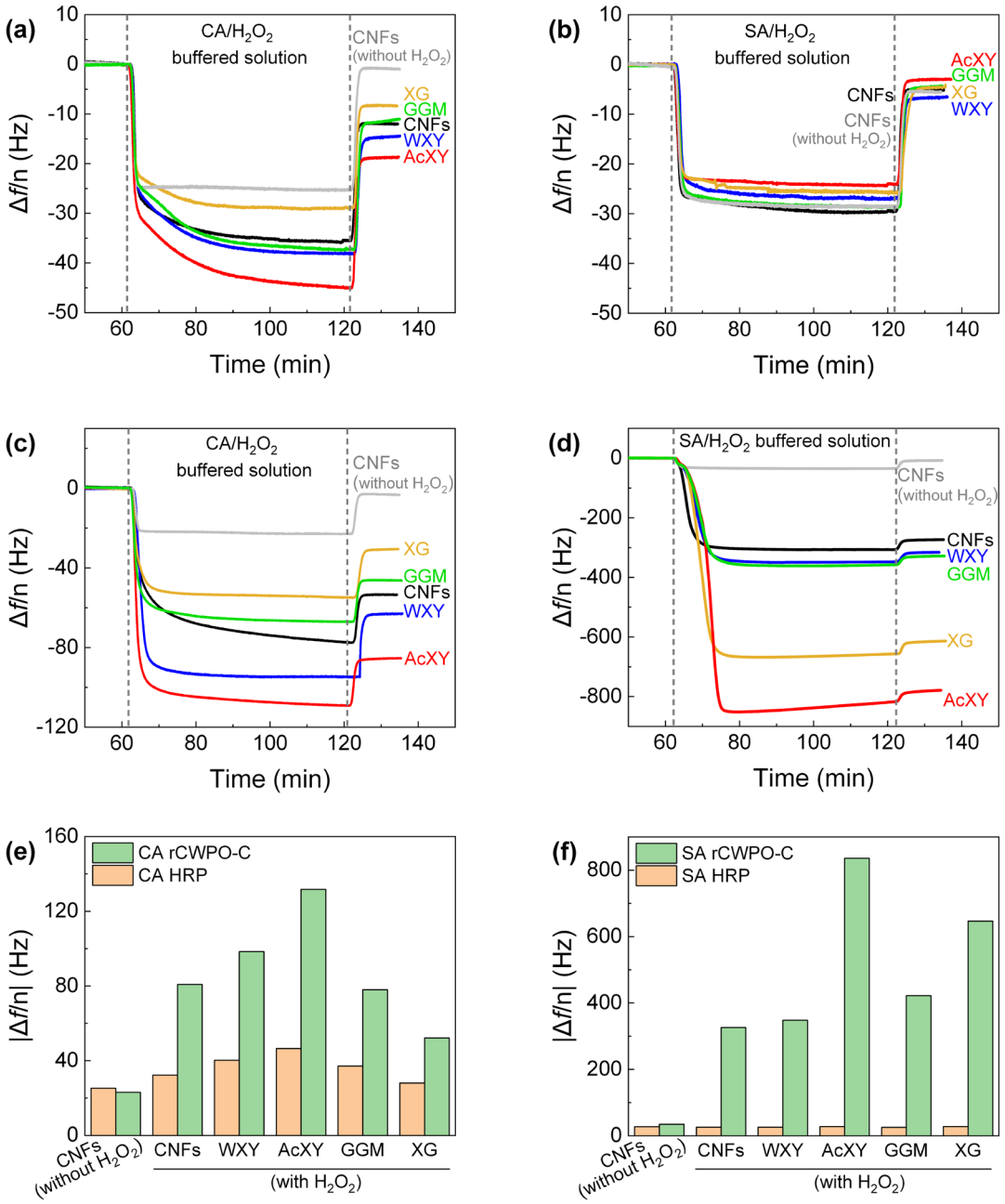

335

336 **Fig. 4.** Δ*f*/n profiles as a function of elution time during the flow of CA (a) and SA (b) buffered
337 solutions on a HRP-adsorbed sensor and during the flow of CA (c) and SA (d) buffered solutions
338 on a rCWPO-C-adsorbed sensor. |Δ*f*/n| values at the smallest Δ*f*/n during flowing CA (e) and SA (f).
339 The sensors were coated with polysaccharides, CNFs, WXY, AcXY, GGM and XG, and the
340 measurements were performed with/without H_2O_2.

341

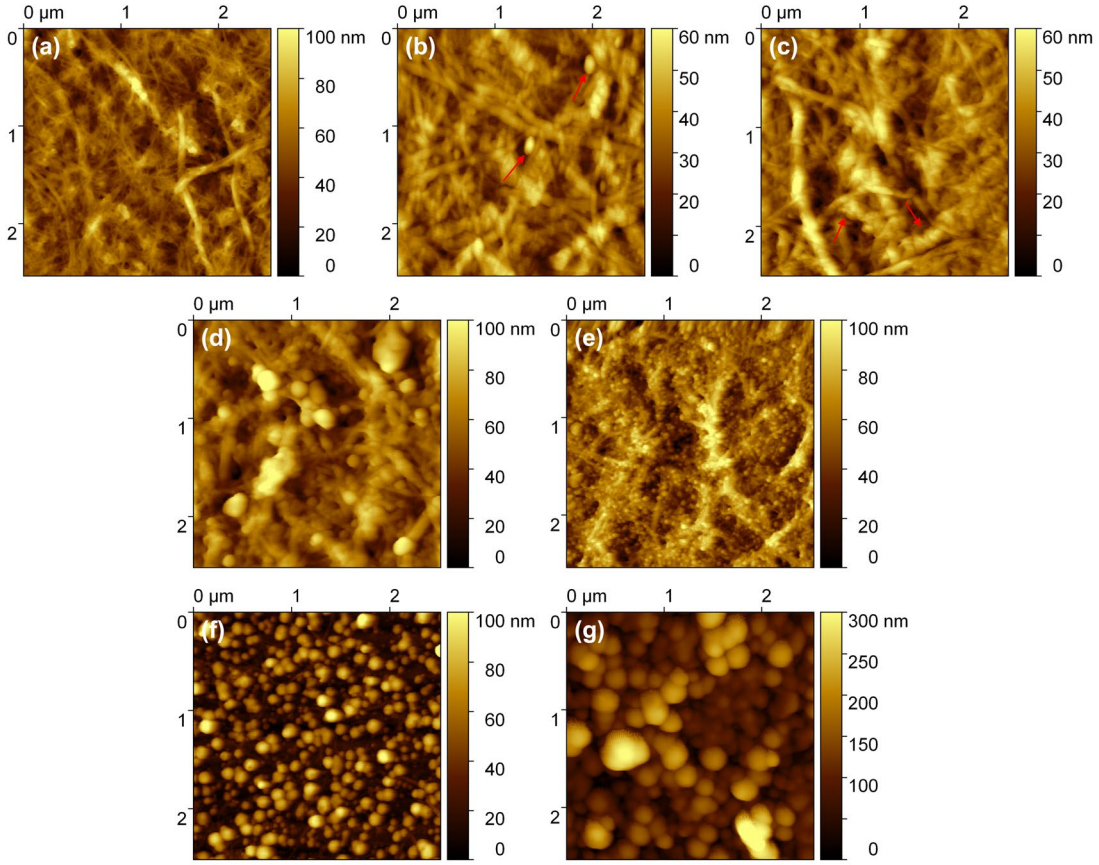

342

343 **Fig. 5.** AFM images of QCM-D sensor surfaces. (a) CNF-coated sensor. (b) CNF- and (c) AcXY-
344 coated HRP-absorbed sensors after flowing CA/H_2O_2, where the formed DHP particles are indicated
345 by arrows. (d) CNF- and (e) AcXY-coated rCWPO-C-absorbed sensors after flowing CA/H_2O_2; (f)
346 CNF- and (g) AcXY-coated rCWPO-C-absorbed sensors after flowing SA/H_2O_2.

347

348 Figure 6 shows the ΔD-Δf/n profiles obtained during DHP formation by rCWPO-C catalysis.
349 For CA flow (Fig. 6a), the profile without H_2O_2 is steeper than other profiles with H_2O_2, suggesting
350 that the sensor surfaces become rigid upon DHP formation with H_2O_2. This can be attributed to
351 expulsion of bound water on the polysaccharide matrix, induced by the formation of hydrophobic
352 DHPs. In particular, the sensor surface with AcXY is more rigid than that with other polysaccharides
353 because the amount of DHP formed in the AcXY matrix is the largest. On the other hand, for SA
354 flow (Fig. 6b), the slopes for all ΔD-Δf/n profiles are almost identical at the initial stage from 0 to -
355 25 Hz of Δf/n, and then, the slopes become less steep at the latter stage. These profiles suggest that

SA adsorption occurs first, and then, the surface becomes rigid as DHP formation proceeds. At the final stage, the surfaces become more rigid, possibly because the DHP densely accumulates onto the sensor. This tendency is more pronounced in the AcXY-coated sensor than in other polysaccharide-coated sensors.

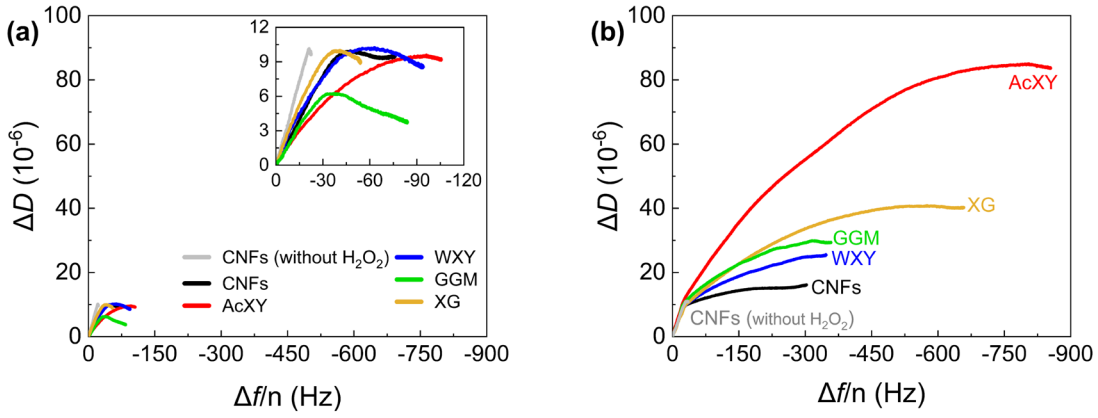

Fig. 6. ΔD *vs.* Δf/n plots for flowing CA (a) and SA (b) buffered solutions with/without H_2O_2 on rCWPO-C-adsorbed sensors coated with polysaccharides.

Based on the above experimental findings, a DHP formation mechanism in the peroxidase-polysaccharide matrix (Fig. 7) is proposed as follows: First, considering that rCWPO-C is adsorbed onto the sensor surface coated with polysaccharides, DHP formation should occur on only the surface. After the formed DHP grows into a spherical particle with a diameter of hundreds of nanometers, it can become detached from the matrix surface. Concomitantly, a new formation of another DHP particle begins at this site. These formed particles associate with each other through several interactions, such as hydrophobic and hydrogen bonding interactions (Uraki et al., 2012). This process occurs successively. Finally, the DHP particles accumulate, as shown in the AFM images (Fig. 5). When the matrix consists of AcXY, it adsorbs a large amount of rCWPO-C through hydrophobic interactions, leading to the formation of a large quantity of DHPs. Furthermore, AcXY also holds the DHP particles through hydrophobic interactions for a longer time than other polysaccharides, which enables the DHP particles to grow to a larger size. Consequently, both the

quantity and particle size of the formed DHPs are the largest on AcXY among those on all polysaccharides.

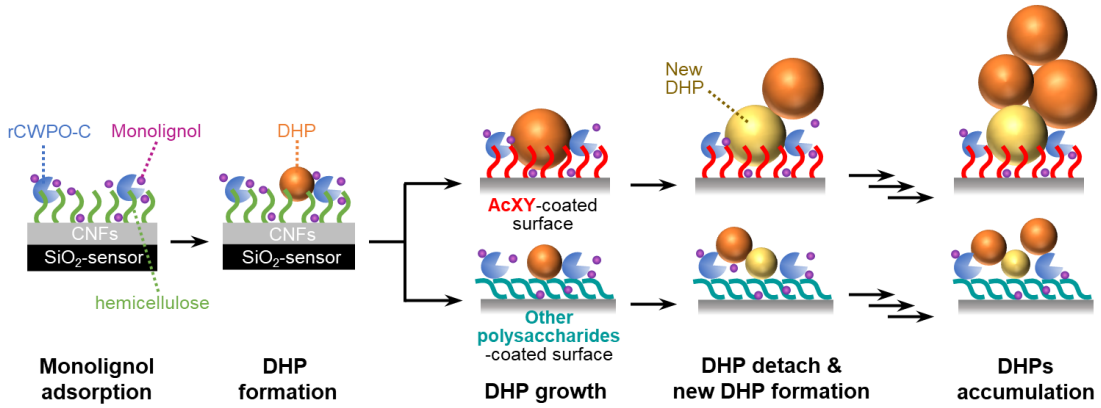

Fig. 7. Proposed mechanism for DHP formation in rCWPO-C-adsorbed polysaccharide matrices.

4. Conclusion

The components in wood cell walls are well known, but the interactions among them and their cooperative functions on lignification have not been clarified. In this study, dehydrogenative polymerization of monolignols catalyzed by a poplar-derived peroxidase, rCWPO-C, in artificial polysaccharide matrices is real-time monitored by using QCM-D. It is found that DHP formation is more facilitated when the matrix contains AcXY than WXY. This result supports our hypothesis that Ac group in native glucuronoxylan would play an important role in hardwood lignification. In addition, a mechanism for the lignification process in hardwood is proposed based on the large amount of rCWPO-C adsorption on AcXY and the development of DHP particles assisted by AcXY. These investigations would be expanded to elucidate the lignification process in softwood because it also contains partially acetylated galactoglucomannan.

CRediT authorship contribution statement

Yan Lyu: Investigation, Formal analysis, Data curation, Writing – original draft. **Shiori Suzuki:** Supervision, Writing – original draft & review & editing. **Hiroki Nagano:** Investigation, Formal

analysis, Resource (AcXY). **Kengo Shigetomi:** Supervision, Writing – review & editing. **Tutaka Tamai:** Resource (GGM & XG). **Yuji Tsutsumi:** Resource (rCWPO-C). **Yasumitsu Uraki:** Conceptualization, Supervision, Project administration, Funding acquisition, Writing – review & editing.

Conflict of interest disclosure

The authors declare no competing interest.

Funding sources

This work was financially supported by a grant-in-aid for Scientific Research (A) (Grant No. 21H04730) from the Japan Society for the Promotion of Science (JSPS).

References

Aoyama, W., Sasaki, S., Matsumura, S., Mitsunaga, T., Hirai, H., Tsutsumi, Y., & Nishida, T. (2002). Sinapyl alcohol-specific peroxidase isoenzyme catalyzes the formation of the dehydrogenative polymer from sinapyl alcohol. *Journal of Wood Science, 48*(6), 497-504.

Busse-Wicher, M., Gomes, T. C., Tryfona, T., Nikolovski, N., Stott, K., Grantham, N. J., Bolam, D. N., Skaf, M. S., & Dupree, P. (2014). The pattern of xylan acetylation suggests xylan may interact with cellulose microfibrils as a twofold helical screw in the secondary plant cell wall of *Arabidopsis thaliana*. *the Plant Journal, 79*(3), 492-506.

Dixon, M. C. (2008). Quartz crystal microbalance with dissipation monitoring: enabling real-time characterization of biological materials and their interactions. *Journal of Biomolecular Techniques, 19*(3), 151-158.

Donaldson, L. A. (1994). Mechanical constraints on lignin deposition during lignification. *Wood Science and Technology, 28*(2), 111-118.

Du, X., Gellerstedt, G., & Li, J. (2013). Universal fractionation of lignin-carbohydrate complexes

(LCCs) from lignocellulosic biomass: an example using spruce wood. *the Plant Journal, 74*(2), 328-338.

Du, X., Perez-Boada, M., Fernandez, C., Rencoret, J., del Rio, J. C., Jimenez-Barbero, J., Li, J., Gutierrez, A., & Martinez, A. T. (2014). Analysis of lignin-carbohydrate and lignin-lignin linkages after hydrolase treatment of xylan-lignin, glucomannan-lignin and glucan-lignin complexes from spruce wood. *Planta, 239*(5), 1079-1090.

Elschner, T., Adam, J., Lesny, H., Joseph, Y., & Fischer, S. (2022). Growing of Artificial Lignin on Cellulose Ferulate Thin Films. *Biomacromolecules, 23*, 2089-2097.

Eronen, P., Österberg, M., Heikkinen, S., Tenkanen, M., & Laine, J. (2011). Interactions of structurally different hemicelluloses with nanofibrillar cellulose. *Carbohydrate Polymers, 86*(3), 1281-1290.

Farooq, M., Zou, T., Valle-Delgado, J. J., Sipponen, M. H., Morits, M., & Osterberg, M. (2020). Well-defined lignin model films from colloidal lignin particles. *Langmuir, 36*(51), 15592-15602.

George, P. (1953). Intermediate compound formation with peroxidase and strong oxidizing agents. *Journal of Biological Chemistry, 201*(1), 413-426.

Giummarella, N., Zhang, L., Henriksson, G., & Lawoko, M. (2016). Structural features of mildly fractionated lignin carbohydrate complexes (LCC) from spruce. *RSC Advances, 6*(48), 42120-42131.

Kabel, M. A., van den Borne, H., Vincken, J.-P., Voragen, A. G. J., & Schols, H. A. (2007). Structural differences of xylans affect their interaction with cellulose. *Carbohydrate Polymers, 69*(1), 94-105.

Li, Q., Koda, K., Yoshinaga, A., Takabe, K., Shimomura, M., Hirai, Y., Tamai, Y., & Uraki, Y. (2015). Dehydrogenative polymerization of coniferyl alcohol in artificial polysaccharides matrices: effects of xylan on the polymerization. *Journal of Agricultural and Food Chemistry, 63*(18), 4613-4620.

448 Littunen, K., Mai-Gisondi, G., Seppälä, J., & Master, E. R. (2017). Enzymatically debranched
449 xylans in graft copolymerization. *Biomacromolecules, 18*(5), 1634-1641.
450 Lyu, Y., Matsumoto, T., Taira, S., Ijiri, K., Yoshinaga, A., Shigetomi, K., & Uraki, Y. (2021).
451 Influences of polysaccharides in wood cell walls on lignification *in vitro*. *Cellulose, 28*(15),
452 9907-9917.
453 Pawar, P. M., Derba-Maceluch, M., Chong, S. L., Gandla, M. L., Bashar, S. S., Sparrman, T.,
454 Ahvenainen, P., Hedenström, M., Özparpucu, M., Rüggeberg, M., Serimaa, R., Lawoko,
455 M., Tenkanen, M., Jönsson, L. J., & Mellerowicz, E. J. (2017). *In muro* deacetylation of
456 xylan affects lignin properties and improves saccharification of aspen wood. *Biotechnology*
457 *Biofuels, 10*, 98.
458 Pawar, P. M., Koutaniemi, S., Tenkanen, M., & Mellerowicz, E. J. (2013). Acetylation of woody
459 lignocellulose: significance and regulation. *frontiers in Plant Science, 4*, 118.
460 Qaseem, M. F., & Wu, A. M. (2020). Balanced xylan acetylation is the key regulator of plant growth
461 and development, and cell wall structure and for industrial utilization. *International Journal*
462 *of Molecular Sciences, 21*(21), 7875.
463 Quideau, S., & Ralph, J. (1992). Facile large-scale synthesis of coniferyl, sinapyl, and *p*-coumaryl
464 alcohol. *Journal of Agricultural and Food Chemistry, 40*(7), 1108-1110.
465 Ralph, J., Brunow, G., & Boerjan, W. (2007). Lignins. *Encyclopedia of Life Sciences*, 1-10.
466 Saake, B., Argyropoulos, D. S., Beinhoff, O., & Faix, O. (1996). A comparison of lignin polymer
467 models (DHPs) and lignins by ^{31}P NMR spectroscopy. *Phytochemistry, 43*(2), 499-507.
468 Sasaki, S., Nishida, T., Tsutsumi, Y., & Kondo, R. (2004). Lignin dehydrogenative polymerization
469 mechanism: a poplar cell wall peroxidase directly oxidizes polymer lignin and produces in
470 vitro dehydrogenative polymer rich in β-*O*-4 linkage. *FEBS Letters, 562*(1-3), 197-201.
471 Sauerbrey, G. (1959). Verwendung von schwingquarzen zur wägung dünner schichten und zur
472 mikrowägung. *Zeitschrift für Physik, 155*(2), 206-222.
473 Shigeto, J., Itoh, Y., Tsutsumi, Y., & Kondo, R. (2012). Identification of Tyr74 and Tyr177 as

474 substrate oxidation sites in cationic cell wall-bound peroxidase from *Populus alba* L. *the*
475 *FEBS Journal, 279*(2), 348-357.
476 Sugiyama, J., Vuong, R., & Chanzy, H. (1991). Electron diffraction study on the two crystalline
477 phases occurring in native cellulose from an algal cell wall. *Macromolecules, 24*, 4168-
478 4175.
479 Taira, S., Tsuruhara, M., Saito, R., Koda, K., Uraki, Y., Konno, H., & Shimamoto, S. (2020).
480 Cellulose acetate with CTA I polymorph can be defibrated into nanofibers to produce a
481 highly transparent nanopaper. *Cellulose, 27*(9), 4991-5001.
482 Teleman, A., Lundqvist, J., Tjerneld, F., Stålbrand, H., & Dahlman, O. (2000). Characterization of
483 acetylated 4-*O*-methylglucuronoxylan isolated from aspen employing ^{1}H and ^{13}C NMR
484 spectroscopy. *Carbohydrate Research, 329*(4), 807-815.
485 Teleman, A., Tenkanen, M., Jacobs, A., & Dahlman, O. (2002). Characterization of *O*-acetyl-(4-*O*-
486 methylglucurono) xylan isolated from birch and beech. *Carbohydrate Research, 337*(4),
487 373-377.
488 Terashima, N., Yoshida, M., Hafrén, J., Fukushima, K., & Westermark, U. (2012). Proposed
489 supramolecular structure of lignin in softwood tracheid compound middle lamella regions.
490 *Holzforschung, 66*(8), 907-915.
491 Uraki, Y., Sugiyama, Y., Koda, K., Kubo, S., Kishimoto, T., & Kadla, J. F. (2012). Thermal mobility
492 of *β*-*O*-4-type artificial lignin. *Biomacromolecules, 13*(3), 867-872.
493 Veitch, N. C. (2004). Horseradish peroxidase: a modern view of a classic enzyme. *Phytochemistry,*
494 *65*(3), 249-259.
495 Wang, C., Qian, C., Roman, M., Glasser, W. G., & Esker, A. R. (2013). Surface-initiated
496 dehydrogenative polymerization of monolignols: a quartz crystal microbalance with
497 dissipation monitoring and atomic force microscopy study. *Biomacromolecules, 14*(11),
498 3964-3972.
499 Wariishi, H., Valli, K., & Gold, M. H. (1992). Manganese(II) oxidation by manganese peroxidase

500 from the basidiomycete *Phanerochaete chrysosporium*. Kinetic mechanism and role of
501 chelators. *Journal of Biological Chemistry, 267*(33), 23688-23695.
502 Warinowski, T., Koutaniemi, S., Kärkönen, A., Sundberg, I., Toikka, M., Simola, L. K., Kilpeläinen,
503 I., & Teeri, T. H. (2016). Peroxidases Bound to the Growing Lignin Polymer Produce
504 Natural Like Extracellular Lignin in a Cell Culture of Norway Spruce. *frontiers in Plant*
505 *Science, 7*, 1523.
506 Wi, S. G., Singh, A. P., Lee, K. H., & Kim, Y. S. (2005). The pattern of distribution of pectin,
507 peroxidase and lignin in the middle lamella of secondary xylem fibres in alfalfa (*Medicago*
508 *sativa*). *Annals of Botany, 95*(5), 863-868.
509 Willför, S., Sundberg, K., Tenkanen, M., & Holmbom, B. (2008). Spruce-derived mannans – A
510 potential raw material for hydrocolloids and novel advanced natural materials.
511 *Carbohydrate Polymers, 72*(2), 197-210.
512 Zhong, R., Cui, D., & Ye, Z. H. (2017). Regiospecific acetylation of xylan is mediated by a group
513 of DUF231-containing *O*-acetyltransferases. *Plant & Cell Physiology, 58*(12), 2126-2138.